

Neural Networks with Dynamical Links and Self-Organized Criticality

João Guilherme Ferreira Campos,^{1,*} Ariadne de Andrade Costa,² Mauro Copelli,¹ and Osame Kinouchi²

¹*Departamento de Física, Universidade Federal de Pernambuco, 50670-901 Recife, PE, Brazil*

²*Departamento de Física, FFCLRP, Universidade de São Paulo, 14040-901, Ribeirão Preto, SP, Brazil*

In a recent work, mean-field analysis and computer simulations were employed to analyze critical self-organization in excitable cellular automata annealed networks, where randomly chosen links were depressed after each spike. Calculations agree with simulations of the annealed version, showing that the nominal *branching ratio* σ converges to unity, and fluctuations vanish in the thermodynamic limit, as expected of a self-organized critical system. However, the question remains whether the same results apply to a biologically more plausible, quenched version, in which the neighborhoods are fixed, and only the active synapses are depressed. We show that simulations of the quenched model yield significant deviations from $\sigma = 1$, due to spatio-temporal correlations. However, the model is shown to be critical, as the largest eigenvalue λ of the synaptic matrix is shown to approach unity, with fluctuations vanishing in the thermodynamic limit.

PACS numbers: 05.65.+b, 05.70.Ln, 07.05.Mh

I. INTRODUCTION

The first empirical evidence of criticality in the brain was given by Beggs and Plenz, who reported that in vitro rat cortex slices exhibit neuronal avalanches with power law distribution with exponents $-3/2$ and -2 for avalanche size and duration, respectively [1]. This was regarded as evidence that the brain as a dynamical system fluctuates around a critical point, presumably similar to a critical branching process with the branching parameter close to unity. Either on theoretical or experimental grounds, this property has been shown to optimize computational capabilities [2], information transmission [1, 3] and sensitivity to stimuli [4–6], among others, as recently reviewed in Refs. [7, 8].

In order to explain the self-organization around the critical point, Levina, Hermann and Geisel (LHG) proposed a model [9] which consists of a fully connected network of integrate and fire neurons, such that when a neuron fires, the strength of its output links (synapses) are reduced by a fraction. This fast dissipation mechanism is associated with short-term synaptic depression due to temporary neurotransmitter depletion. It is countered by a loading mechanism at a different time scale, by which synaptic neurotransmitters are slowly replenished when the synapse is idle. LHG claimed their model exhibit Self-Organized Criticality (SOC), based on the emergence of power-law distributions of avalanche sizes.

On a pair of review papers, however, Bonachela *et al.* showed that for a system to exhibit SOC its bulk dynamics must be conservative at least in average [10–12]. They showed that systems with dissipative and loading mechanisms such as the LHG model would hover around the critical point. In that sense, the behavior of the LHG model would not be classified as SOC, but rather was called Self Organized quasi-Criticality (SOqC).

In a recent work, we analyzed a random neighbor network of excitable cellular automata with dynamical synapses [13]. It was based on the LHG model, but with three different ingredients: finite connectivity (with K outgoing synapses in a random graph), discrete units and multiplicative probabilistic synapses. In its annealed version, K randomly chosen synapses are depressed whenever any neuron spikes. The model was shown to behave differently from the LHG model, in that not only did the nominal branching ratio σ converged to unity but, perhaps most importantly, the fluctuations around the criticality condition $\sigma = 1$ vanished in the thermodynamic limit.

Despite the agreement between the mean-field calculations and the numerical simulations, a major drawback of the annealed model is its lack biological plausibility. Here we investigate in detail the quenched version of the model, in which when a presynaptic neuron fires, its outgoing synapses are depressed. In particular, we focus on whether the quenched model behaves similarly to the annealed model as far as SOC is concerned.

The rest of the paper is structured as follows. In section 2, we revisit the model, and in particular the differences between annealed and quenched networks. In section 3, we present our simulation results and discussions. Concluding remarks appear in section 4.

II. THE MODEL

Our model builds upon a random-neighbor network of excitable neurons (quiescent ($S_j = 0$), to firing ($S_j = 1$), to refractory ($S_j = 2, 3, \dots, n - 1$), to quiescent ($S_j = 0$, $j = 1, \dots, N$)) automata used previously [4, 13]. In this version, N sites with states $S_j(t)$ have each exactly $K_j^{out} = K$ outlinks to post-synaptic neurons $S_i(t)$ coupled via probabilistic synapses $P_{ij}(t)$, which define a connectivity matrix. With this construction, each neuron has K_j^{in} binomially distributed incoming links with average K . After a site spikes, it deterministically becomes

* joaogfc@gmail.com

refractory for $n-2$ time steps [$S_j(t+2) = 2, S_j(t+3) = 3, \dots, S_j(t+n-1) = n-1$] and then returns to quiescence (for details, see Ref. [13]). On the quenched case, the synapses are dynamic and their evolution obeys the following equation:

$$P_{ij}(t+1) = P_{ij}(t) + \frac{\epsilon}{KN}(A - P_{ij}(t)) - uP_{ij}(t)\delta(t - t_j), \quad (1)$$

where ϵ is the coefficient of synaptic recovery, A the asymptotic synaptic value and u is the fraction of synaptic coupling that is lost whenever a neuron fires. The $\{t_j\}$ are the time intervals when the neuron j fires, which means that, whenever a neuron fires, all its outgoing synapses are reduced to $(1-u)$ of their original value.

On the other hand, for annealed networks, instead of depressing the K outgoing synapses of a given neuron, either K randomly chosen synapses are depressed after a given spike or a random neuron is chosen and its K outgoing synapses are depressed after a given spike. The purpose of the annealed case is to destroy correlations between the P_{ij} , so one can use mean-field analysis to get a better insight of the problem, as done previously [13]. Both annealed cases work equally well in destroying correlations, but the latter is more computationally efficient.

The initial conditions for the synapses are defined by choosing σ_0 and uniformly drawing random values to $P_{ij}(0)$ in the interval $[0, \frac{2\sigma_0}{K}]$. The system is set in the slow driving limit. The initial condition is $S_i(0) = 0$ for all $i \neq k$ and $S_k(0) = 1$, i. e., we start an avalanche at site k . Whenever the system returns to quiescence (that is, the absorbing state $S_i(t) = 0, \forall i$), we start another avalanche, for all i , by choosing a random neuron l , and setting $S_l(t+1) = 1$.

We let the system evolve and after a transient period it approaches a stationary state. At each time step we compute a local branching ratio $\sigma_j(t) = \sum_i^K P_{ij}(t)$ and a global branching ratio $\sigma(t) = \frac{1}{N} \sum_{j=1}^N \sigma_j(t)$. In the stationary state, $\sigma(t)$ oscillates around some average value σ^* with dispersion $\Delta\sigma^*$. As shown in [13], the mean-field analysis predicts that:

$$\sigma^* - 1 \simeq \frac{(AK - 1)}{1 + x}, \quad (2)$$

where $x \equiv \frac{uKN}{(n-1)}\epsilon$. So for $N \gg (n-1)/uK\epsilon$

$$\sigma^* - 1 \simeq \frac{\Omega}{N}, \quad (3)$$

where $\Omega \equiv \frac{(AK-1)(n-1)}{uK\epsilon}$. That is, the mean-field analysis predicts that, for large N , σ^* differs from $\sigma_c = 1$ by a factor of order $\frac{1}{N}$, therefore $\sigma^* = 1$ in the infinite-size limit.

We define the Perron-Frobenius (largest) eigenvalue of the connectivity matrix $P_{ij}(t)$ as $\lambda(t)$, which in the stationary state oscillates around the mean value λ^* with dispersion $\Delta\lambda^*$. As shown previously by Larremore et al. [14], the phase transition between an absorbing and

an active phases occurs at $\lambda = 1$. The question then arises: does the quenched model converges to $\lambda^* = 1$ and, if so, how does the fluctuations behave?

In the next section, we analyze the behavior of λ^* and σ^* , and their respective dispersions, with our model parameters ϵ, u, A, K , as a function of N .

III. SIMULATION RESULTS

To simplify our simulations we fix $K = 10$, meaning that the number of outgoing synapses is much smaller than the number of neurons. If we fix ϵ and plot σ^* and λ^* while we vary N , we obtain Fig. 1. Observe in Fig. 1a that, for annealed networks, when ϵ is small, σ^* is smaller than 1 and is independent of N ; but as ϵ increases, σ^* also increases until it starts behaving like Eq. 3 for $\epsilon \gtrsim 8$. For these values of ϵ , we also plot in Fig. 1a the curves predicted by Eq. 3.

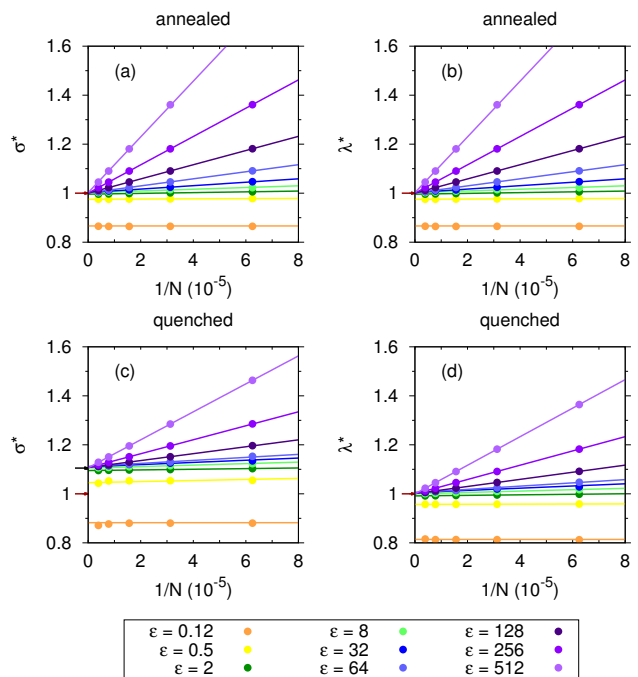


FIG. 1. σ^* and λ^* versus $1/N$ for several values of ϵ for quenched and annealed networks. The error bars do not appear in this scale. The lines are curves of the type $f(N) = A + B/N$ that best fit the data, except for (a) where the curves are the given by Eq. 3 for $\epsilon \geq 8$. Parameters: $n = 3, K = 10, A = 1.0, u = 0.1$.

For quenched networks, the behavior is quite similar, as shown in Fig. 1c. However, as we increase ϵ , σ^* behaves as

$$\sigma^* - 1.105 \simeq \frac{\beta}{N}, \quad (4)$$

for some constant β , instead of following Eq. 3. That indicates that mean-field theory does not describe well

the quenched case. Furthermore, if we fix N and vary ϵ , as in Fig. 2, we see that for annealed networks (Fig. 2a) $\sigma^* \approx 1$ for a wide range of the parameter values that gets bigger as N increases. However for quenched networks (Fig. 2c) we see the same behavior with $\sigma^* \approx 1.105$ instead of 1. The same apparently strange behavior of quenched networks does not appear in the plots for λ^* shown in Fig. 1d and 2d. This occurs because σ^* is the wrong “control” parameter: λ^* is the correct predictor for criticality, as shown by Larremore *et al.* [14].

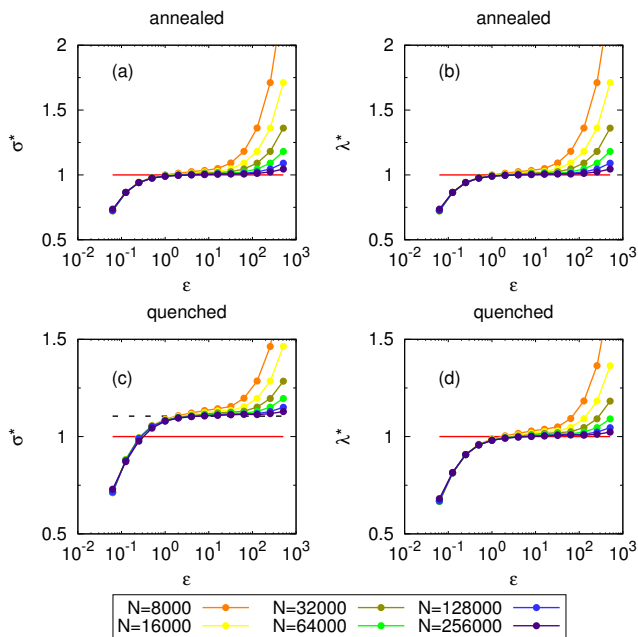


FIG. 2. σ^* and λ^* versus ϵ for several values of N for quenched and annealed networks. The error bars do not appear in this scale. The red line is the critical value 1 and the dashed line is 1.105. The other lines are guides to the eye. Parameters: $n = 3$, $K = 10$, $A = 1.0$, $u = 0.1$.

If we plot λ^* versus σ^* for all the simulations shown in Figs. 1 and 2 we get Fig. 3. Notice that for quenched networks we obtain $\sigma^* = 1.105$ exactly when $\lambda^* = 1$ (see Fig. 3), meaning that λ^* indeed approaches a critical value in quenched networks (see Fig. 1 and 2). Moreover, in the annealed networks the points lie exactly in the identity curve (see Fig. 3). This is consistent with the known result that the equality $\sigma = \lambda$ holds only when there are no correlations between the P_{ij} (see [14]).

In Fig. 1 we see that all curves are straight lines. Thus, aiming at understanding the behavior of the networks as $N \rightarrow \infty$, we fit the data with curves of the type $f_\sigma(N) = \alpha_\sigma + \frac{\beta_\sigma}{N}$ and $f_\lambda(N) = \alpha_\lambda + \frac{\beta_\lambda}{N}$ for σ^* and λ^* , respectively, as shown in Fig. 1 (except for σ^* for $\epsilon \geq 8$ in the annealed case, where we show the theoretical curve). We also observe that $\lim_{N \rightarrow \infty} \sigma^* = \alpha_\sigma$ and $\lim_{N \rightarrow \infty} \lambda^* = \alpha_\lambda$ and plot them as a function of ϵ . The result is shown in Fig. 4.

For annealed networks and $\epsilon \gtrsim 4$, we obtain

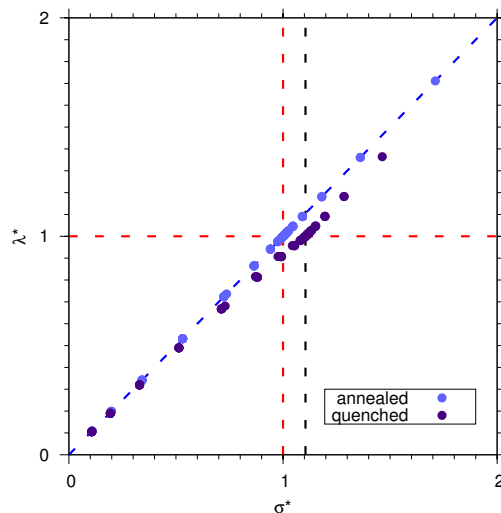


FIG. 3. λ^* versus σ^* for several values of N and ϵ for quenched and annealed networks. The red dashed line is $\lambda^* = 1$, the blue dashed line is the identity function $\lambda^* = \sigma^*$ and the black dashed line is $\sigma^* = 1.105$. Parameters: $n = 3$, $K = 10$, $A = 1.0$, $u = 0.1$.

$\lim_{N \rightarrow \infty} \sigma^* = 1$, within errors (Fig. 4a). For quenched networks and $\epsilon \gtrsim 8$, we obtain $\lim_{N \rightarrow \infty} \sigma^* = 1.105$, within errors (Fig. 4c). On the other hand, $\lim_{N \rightarrow \infty} \lambda^* = 1$, within errors, for $\epsilon \gtrsim 4$ (annealed, Fig. 4b) and $\epsilon \gtrsim 8$ (quenched, Fig. 4d). That is, quenched (annealed) networks are either subcritical, if $\epsilon \lesssim 8$ ($\epsilon \lesssim 4$), or critical, if $\epsilon \gtrsim 8$ ($\epsilon \gtrsim 4$), in the infinite size limit, but never supercritical. This means that there is a semi-infinite volume in the (ϵ, A, u) parameter space with critical α_λ . This is one of the most important results of the paper.

In the following, we present the study of the influence of parameter A for σ^* and λ^* values, for different network sizes (Fig. 5). A single point ($A = 0.1$) did not converge to criticality. It occurs because in the synaptic dynamic we have $(A - P_{ij})$, which implies that $P_{ij} \rightarrow A$ in the limit of no activity. Since we need $P_{ij} = 1/K$ to achieve critical avalanches, A must satisfy $A > 1/K = 0.1$. Lower values of A take the network to subcritical states regardless of ϵ and u .

In Fig. 6 we exhibit the variation of σ^* and λ^* as a function of u . We can see that in both models σ^*, λ^* decreases with u , as expected. It is notable that λ^* converges to 1 for every u as the system size is increased.

Interesting results are also obtained by studying the dependence on the number of neighbors (K). Fig. 7 reveals that the σ^* dependency with K is stronger for the quenched model, whereas variations of λ^* are similar for both models. For increasing K , the systems approach a complete graph.

Now that we understand that $\lambda^* \rightarrow 1$ when $N \rightarrow \infty$ for both networks, we focus on the quenched ones. In Fig. 8 we plot λ_t versus t , starting from different initial conditions for λ_0 . We see that irrespective of the initial

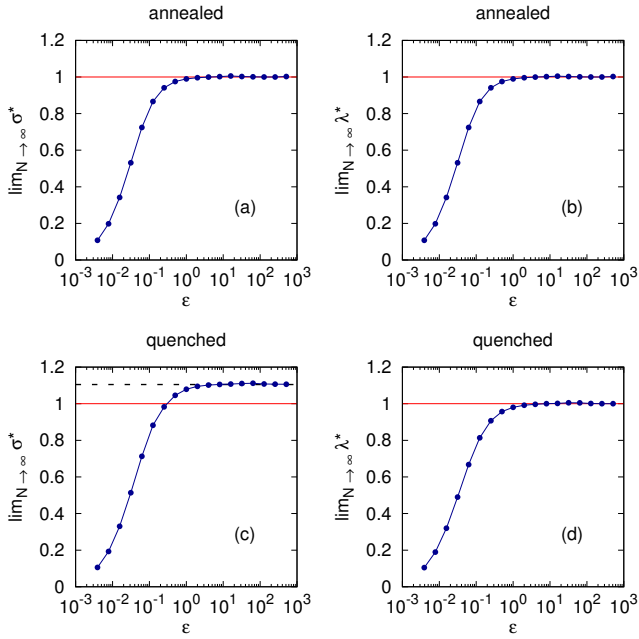


FIG. 4. The limit of σ^* and λ^* when N goes to infinity versus the parameter ϵ for quenched and annealed networks. The red line is the critical value 1 and the dashed line is 1.105. The blue line is a guide to the eye. Parameters: $n = 3$, $K = 10$, $A = 1.0$, $u = 0.1$.

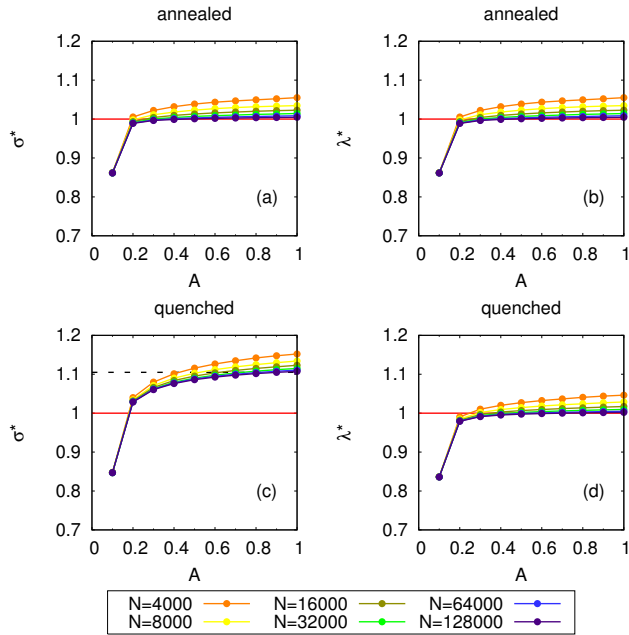


FIG. 5. σ^* and λ^* versus A as N increases, for quenched and annealed networks. The error bars do not appear in this scale. The red line is the critical value 1 and the dashed line is 1.105. Parameters: $\epsilon = 8$, $n = 3$, $K = 10$, $u = 0.1$.

conditions, the network self-organizes its λ_t towards the critical value $\lambda^* \approx \lambda_c = 1$.

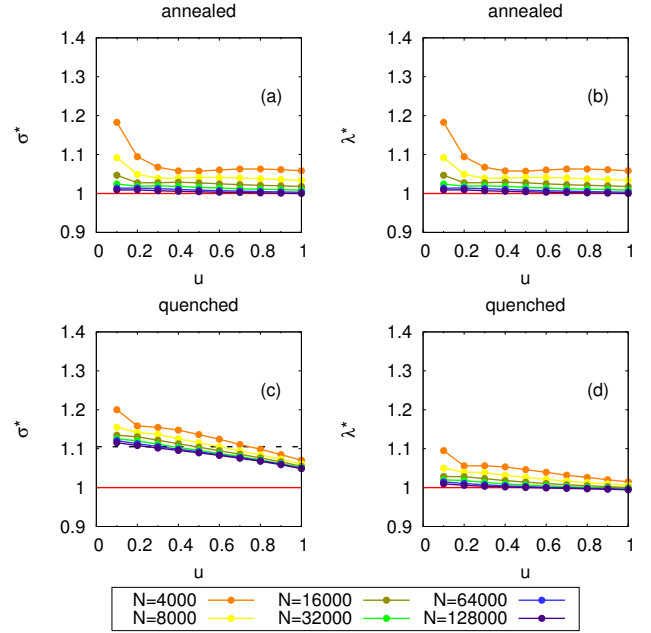


FIG. 6. σ^* and λ^* versus u as N increases, for quenched and annealed networks. The error bars do not appear in this scale. The red line is the critical value 1 and the dashed line is 1.105. The other lines are guides to the eye. Parameters: $\epsilon = 32$, $n = 3$, $K = 10$, $A = 1.0$.

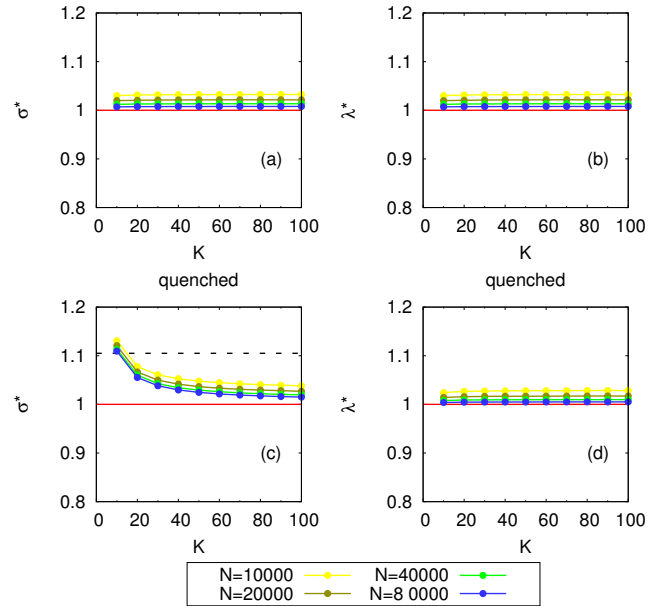


FIG. 7. σ^* and λ^* versus K as N increases. The error bars do not appear in this scale. The red line is the critical value 1 and the dashed line is 1.105. The other lines are guides to the eye. Parameters: $\epsilon = 8$, $n = 3$, $A = 1.0$, $u = 0.1$.

In Fig. 9 we present histograms for λ_t as a function of N by using the scaling $\epsilon \propto N^{1/3}$ suggested by Bonachela *et al.* [11]. The data is collected every 100 timesteps

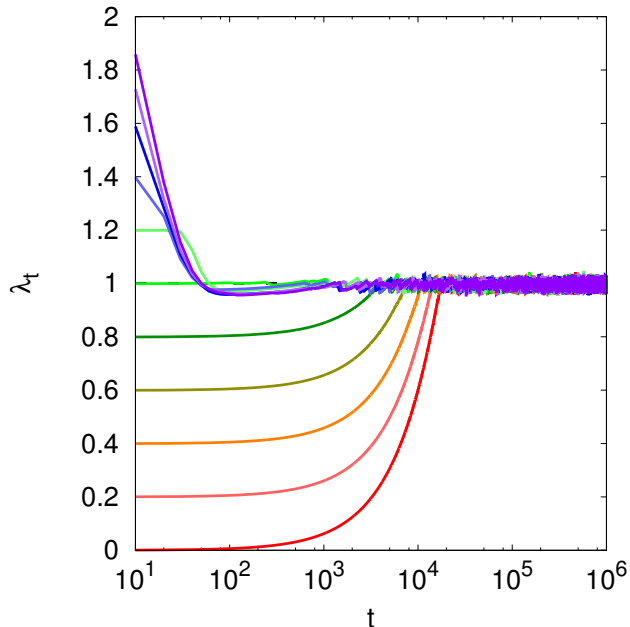


FIG. 8. Evolution of λ_t versus t_N for several different initial values. All curves reach a stationary mean value after a transient time. Parameters: $N = 32000$, $\epsilon = 2$, $n = 3$, $K = 10$, $A = 1.0$, $u = 0.1$.

during a time span of 10^6 , after a transient. We see that the histograms converge to a delta function as N grows, so we have a good SOC behavior similar to conservative models with static parameters. In Fig. 10 we present similar histograms for λ_t but now with fixed ϵ . We see that the behavior toward a delta function also appears even with fixed ϵ . However, for $\epsilon = 64$ this is not so apparent because N is not sufficiently large.

Therefore, we conclude that the fluctuations of $\lambda(t)$ around the mean value vanish in the infinite-size limit. This, together with the fact that $\lambda^* \rightarrow 1$ when $N \rightarrow \infty$, is the most important result of the paper.

IV. CONCLUSION

The nominal branching ratio σ is a good predictor of criticality only for annealed networks, whose definition is such that correlations are destroyed by construction. If σ is used to assess criticality in quenched networks, it incorrectly predicts supercriticality. The largest eigenvalue λ of the synaptic matrix, on the other hand, is a better predictor of criticality than σ , in that it is robust against correlations [14]. When the proposed mechanism of synaptic depression, Eq. (1), is tested with λ instead of σ , it consistently points to a convergence to a self-organized critical regime, for annealed as well as for quenched networks.

Intensive numerical simulations have been employed and the data have been carefully analyzed leading us to

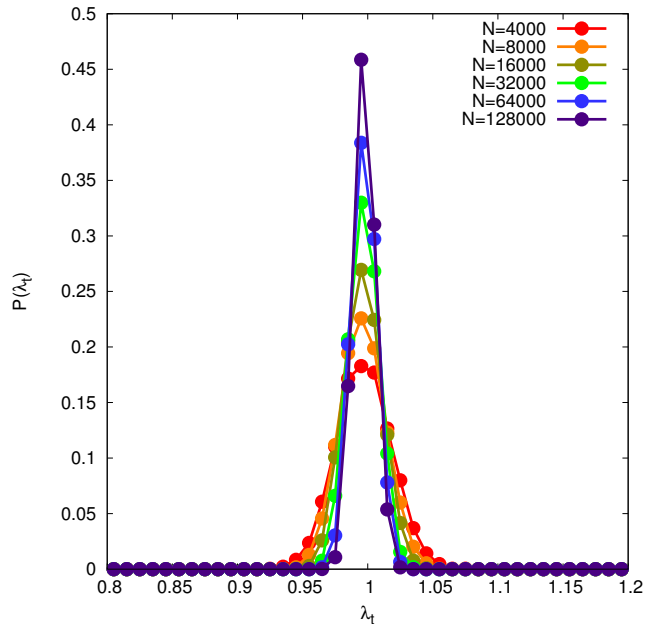


FIG. 9. Histograms of λ_t for quenched networks with $\epsilon = 0.07N^{1/3}$. The lines are guides to the eye. Parameters: $n = 3$, $K = 10$, $A = 1.0$, $u = 0.1$.

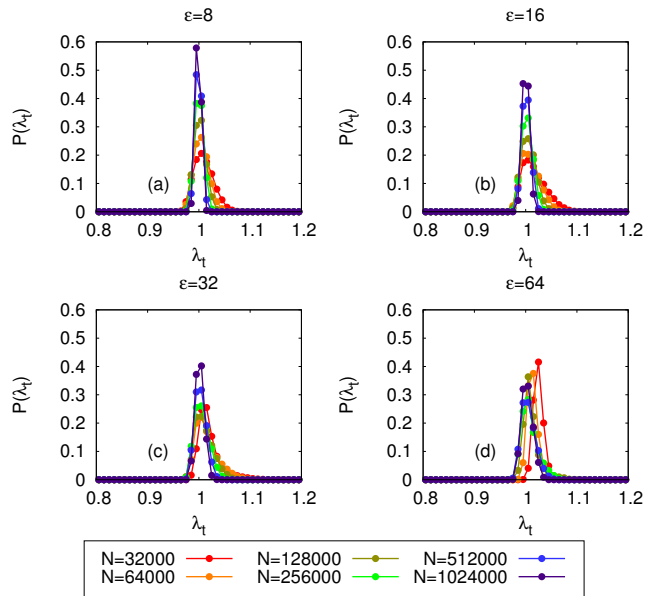


FIG. 10. Histograms of λ_t for quenched networks with fixed $\epsilon = 8, 16, 32$ and 64 . The lines are guides to the eye. Parameters: $n = 3$, $K = 10$, $A = 1.0$, $u = 0.1$.

the conclusion that if the synapses recover fast enough (large enough ϵ), quenched networks are critical in the infinite-size limit. Besides that, in this limit, the fluctuations around the mean value vanish, which means that large enough networks will be indistinguishable from critical ones. So, the mean-field calculation and the simula-

tions both suggest that there is a semi-infinite volume in the parameter space (ϵ, A, u) that produces SOC behavior in the infinite size limit.

CNAIPS-USP, and FAPESP Research, Innovation and Dissemination Center for Neuromathematics (grant #2013/ 07699-0, S. Paulo Research Foundation).

ACKNOWLEDGMENTS

We acknowledge financial support from CAPES, CNPq, PRONEX/FACEPE, PRONEM/FACEPE,

-
- [1] J. M. Beggs and D. Plenz, *J. Neurosci.* **23**, 11167 (2003).
 - [2] N. Bertschinger and T. Natschläger, *Neural Comput.* **16**, 1413 (2004).
 - [3] W. L. Shew, H. Yang, S. Yu, R. Roy, and D. Plenz, *J. Neurosci.* **31**, 55 (2011).
 - [4] O. Kinouchi and M. Copelli, *Nat. Phys.* **2**, 348 (2006).
 - [5] W. Shew, H. Yang, T. Petermann, R. Roy, and D. Plenz, *J. Neurosci.* **29**, 15595 (2009).
 - [6] S. H. Gautam, T. T. Hoang, K. McClanahan, S. K. Grady, and W. L. Shew, *PLoS Comput Biol* **11**, 1 (2015).
 - [7] D. R. Chialvo, *Nat. Phys.* **6**, 744 (2010).
 - [8] W. Shew and D. Plenz, *Neuroscientist* **19**, 88 (2013).
 - [9] A. Levina, J. M. Herrmann, and T. Geisel, *Nat. Phys.* **3**, 857 (2007).
 - [10] J. A. Bonachela and M. A. Muñoz, *J. Stat. Mech.* **2009**, P09009 (2009).
 - [11] J. A. Bonachela, S. de Franciscis, J. J. Torres, and M. A. Muñoz, *J. Stat. Mech.* **2010**, P02015 (2010).
 - [12] S. A. Moosavi and A. Montakhab, *Phys. Rev. E* **89**, 052139 (2014).
 - [13] A. A. Costa, M. Copelli, and O. Kinouchi, *J. Stat. Mech.* **2015**, P06004 (2015).
 - [14] D. Larremore, W. Shew, and J. Restrepo, *Phys. Rev. Lett.* **106**, 058101 (2011).